

## Accepted Article

**Title:** RhIAr/AuIAr' Transmetalation, a Case of Group Exchange  
Pivoting on Formation of M–M' Bonds via Oxidative Insertion

**Authors:** Pablo Espinet, Marconi N. Peñas-Defrutos, Camino  
Bartolomé, and Maximiliano García-Melchor

This manuscript has been accepted after peer review and appears as an Accepted Article online prior to editing, proofing, and formal publication of the final Version of Record (VoR). This work is currently citable by using the Digital Object Identifier (DOI) given below. The VoR will be published online in Early View as soon as possible and may be different to this Accepted Article as a result of editing. Readers should obtain the VoR from the journal website shown below when it is published to ensure accuracy of information. The authors are responsible for the content of this Accepted Article.

**To be cited as:** *Angew. Chem. Int. Ed.* 10.1002/anie.201813419  
*Angew. Chem.* 10.1002/ange.201813419

**Link to VoR:** <http://dx.doi.org/10.1002/anie.201813419>  
<http://dx.doi.org/10.1002/ange.201813419>



regenerated by the reverse reaction at increasing rate as the system approaches the equilibrium. Fortunately, working at 284 K the aryl exchange studied here has an appropriate rate for very precise monitoring, and the initial rate method can be applied within margins of negligible influence of the reverse reaction (consumption of reactants **1** and **2** lower than 10%), to obtain an experimental value of the initial rate ( $r_0$ ).<sup>8</sup> The integrals of well-separated signals, *i.e.* the decreasing  $F_{\text{ortho}}$  signal of reactant **2** (doublet for  $F_{\text{ortho}}\text{-Rh}$  coupling) and the rising sharp  $F_{\text{para}}$  signal of product **3**, were monitored. Additional experiments using different Au:Rh ratios confirmed a kinetic reaction order 1 on the concentration of both metal complexes, as expected (details in SI). Least squares adjustment using these data (Figure 2a) yielded a reaction rate  $r_0 = 1.08 \times 10^{-7} \text{ mol L}^{-1} \text{ s}^{-1}$ . In a simple process this would correspond to an activation Gibbs energy of  $\Delta G_{\text{initial}}^\ddagger = 20.6 \text{ kcal mol}^{-1}$  for a single rate determining step. However this is not a correct interpretation for the more complex mechanism operating here, as discussed below. The kinetic effect of added free arsine ligand on the initial reaction rate was then quantified by measuring the decelerating effect upon addition of different percentages of  $\text{AsPh}_3$  (from 5% to 250%), yielding a ligand dependence  $[\text{AsPh}_3]^{-0.53}$  (Figure 2b).<sup>9,10</sup>

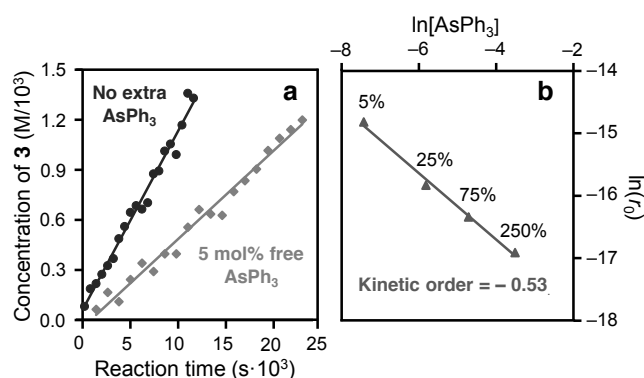


**Figure 2.** (a) Kinetic plot for the reaction between **1** and **2** in THF at 284K, with (black circles) and without (grey squares) excess of free arsine (+ 5%  $\text{AsPh}_3$ ). (b) Change in  $r_0$  upon addition of different amounts of free  $\text{AsPh}_3$  at 298 K.

The high computed DFT Gibbs energies (wb97xd level in THF, at the experimental temperature of 284 K and 1 atm) for  $\text{AsPh}_3$  dissociation from the starting square-planar Rh<sup>I</sup> complex **2** (27.1 kcal mol<sup>-1</sup>) or from the Au<sup>I</sup> complex **1** (31.5 kcal mol<sup>-1</sup>) allow us to discard these potentially initial routes as the origin of  $[\text{AsPh}_3]$  dependence. Moreover, the addition of only 5%  $\text{AsPh}_3$  ligand already results in a large decrease of the reaction rate by a factor of 0.52 (Figure 2a), suggesting that added  $\text{AsPh}_3$  is operating on some lower concentration intermediate and not on **1** or **2**. The data point towards a mechanism far from the *rate-determining step* oversimplification,<sup>11</sup> and support that the kinetics observed must depend on more than one transition state.

For a closer examination of the problem, multivariate kinetic analysis using COPASI,<sup>12</sup> and DFT calculations were used (see SI for details). With new data in hand, a reversible reaction path that fits very well all the experimental observations could be proposed (Figure 3). The profile combines: 1) computed transition states and intermediates by means of DFT

calculations (black lines);<sup>13</sup> 2) plausible structures, with COPASI-adjusted energies (grey and hashed lines). The COPASI adjustment leads to an  $\text{AsPh}_3$  kinetic dependence  $[\text{AsPh}_3]^{-0.64}$ , very close to the experimental value. Since the energy profile is very symmetric, only the first half is discussed.

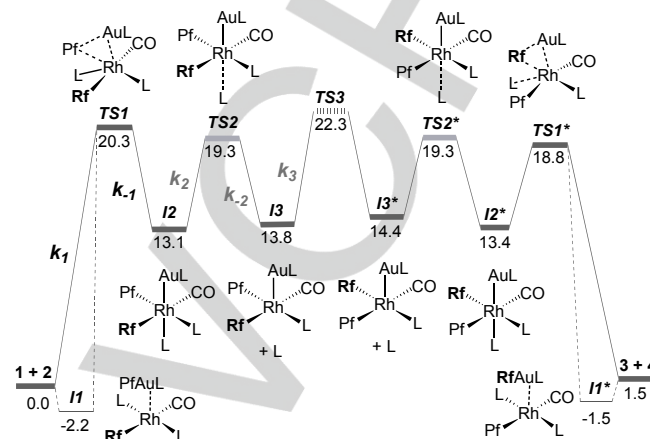


**Figure 3.** Gibbs energy profile for the transmetalation reaction between **1** and **2**, in THF at 284 K and 1 atm.

Beginning in complexes **1** and **2**, DFT simulations found a van der Waals complex **I1** (grey thin line), which is non-existing in solution in the presence of solvating THF molecules. Otherwise, being **I1** hypothetically more stable than **1** and **2**, it should be observed experimentally. Artifacts of this kind may arise in simulations in the absence of explicit solvent molecules and hence, must be discarded (unless experimentally observed) to calculate  $\Delta G^\ddagger$ .

The process starts with the oxidative addition of the Au–Pf bond to Rh, *via* the transition state **TS1**. This first step requires an energy barrier of 20.3 kcal mol<sup>-1</sup> and gives rise to the octahedral complex **I2**, where the Au atom is in the axial position and the Pf moiety is in the equatorial plane, in *cis* position to the Rf group. From **I2**, calculations indicate that the dissociation of the arsine ligand in the axial position to afford the 5-coordinate intermediate **I3** is almost thermoneutral. The corresponding transition state (**TS2**) is barrierless in gas phase (see Figure S13) and was not found, which is frequent for L dissociations by progressive bond elongation (Figure S13). Estimations of coordination transition states in the literature suggest a reasonable value about 4.5 kcal mol<sup>-1</sup> higher than **I3**, due to diffusion cost in solution.<sup>14</sup> The value proposed in the profile, calculated by kinetic COPASI adjustment, is 19.3 kcal mol<sup>-1</sup>, that is 5.5 kcal mol<sup>-1</sup> higher than **I3** (see details in SI). This is an excellent fitting with the literature expectations. Finally, the process requires isomerization from the 5-coordinate species **I3** to **I3\*** before the rest of the process progresses symmetrically. The isomerization of 5-coordinate species has been extensively theoretically studied showing that many reaction pathways are possible with activation energies within 10 kcal mol<sup>-1</sup>.<sup>15</sup> Using COPASI, we estimated the energy of the transition state for (**TS3**) to be 8.5 kcal mol<sup>-1</sup> higher than **I3** ( $\Delta G^\ddagger = 22.3 \text{ kcal mol}^{-1}$ ).

It is worth noting that the  $\text{AsPh}_3$  dissociation barrier for the octahedral complex **I2** is considerably lower than calculated for the square-planar precursor. This can be rationalized considering that the *trans*-influence of the different ligands is  $\text{LAu}^- > \text{Pf} > \text{AsPh}_3$ , which is supported by the order of Rh–As bond distances in complexes **2** and **I2**: ( $\text{Rh–As}_{\text{trans to Au}} = 2.688 \text{ \AA}$  in **I2**)  $>$  ( $\text{Rh–As}_{\text{trans to Pf}} = 2.520 \text{ \AA}$  in **I2**)  $>$  ( $\text{Rh–As}_{\text{trans to As}} = 2.421 \text{ \AA}$  in **2**). Thus, the M–M bond strongly facilitates the dissociation of the ligand in *trans*.

The large effect on the reaction rate of a small amount of added  $\text{AsPh}_3$  is now easily understood observing that the arsine operates on the dissociative step from **I2** to **I3** via **TS1**: the 5% of arsine relative to the initial concentration of complexes **1** and **2** is, in fact, an enormous excess relative to the concentrations of **I2** or **I3** in equilibrium.<sup>16</sup> Indeed, the correct interpretation of the  $\text{AsPh}_3/\mathbf{2} \approx 0.05$  concentration ratio (corresponding in fact to  $\text{AsPh}_3/\mathbf{I2} \approx 10^{11}$  at the correct reaction point) indicates that added  $\text{AsPh}_3$  is very inefficient at preventing its dissociation from **I2**. In other words,  $\text{AsPh}_3$  *trans* to Au( $\text{AsPh}_3$ ) behaves as a very weak ligand (which is consistent with the close energies of **I2** and **I3**), and also as fairly labile ( $\Delta G^\ddagger = 5.5 \text{ kcal mol}^{-1}$  from **I2**).

The combined DFT plus experimental energy profile in Figure 3 illustrates how the Rh<sup>I</sup>Rf/Au<sup>I</sup>Pf exchange occurs through different coordination geometries (square-planar, octahedral and square pyramidal), different oxidation states for the Rh and Au centers, and an isomerization process via 5-coordinate intermediates. Geometrical details of the evolution from the initial square-planar Rh<sup>I</sup> complex **2** (including **I1** for comparison) are summarized in Figure 4. It clearly shows a parallel approximation of the Pf–AuL bond over the L–Rh–L axis, which induces progressive closure of the L–Rh–L angle and concomitant elongation of the Pf–AuL bond in **TS1**. This eventually results in the *cis*-addition of the Pf and AuL groups to complex **2**, giving rise to the octahedral complex **I2**. At this point the high *trans*-influence of the AuL group facilitates dissociation of the  $\text{AsPh}_3$  ligand in *trans*, giving the 5-coordinate **I3** from which isomerization occurs. The formation of the two other possible octahedral isomers arising from approximation of the Pf–AuL bond along the Rf–Rh–CO direction (two possible orientations) was also considered but were discarded based on their high computed activation energies (more than 10 kcal mol<sup>-1</sup> higher than **TS1**, see SI for details).

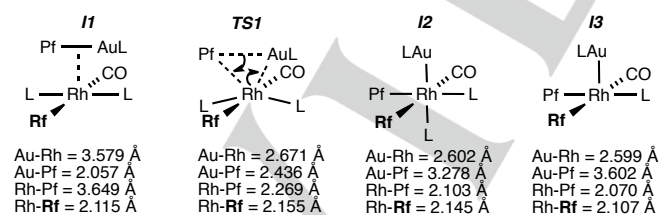


**Figure 4.** Evolution of bond distances along the reaction pathway. **Sum of covalent radii:** Au–Rh = 2.78 Å; Au–C = 2.09 Å; Rh–C = 2.15 Å.

To gain a deeper insight into the energy contributions in **TS1**, we performed an activation-strain analysis,<sup>17</sup> where the total energy is decomposed as  $E = E_{\text{dist}} + E_{\text{int}}$ . The first term,  $E_{\text{dist}}$ , is the so-called *distortion energy* and accounts for the energy cost associated with the geometric distortion of the Au and Rh

fragments (**1** and **2**, respectively) from their structure as isolated species to their “strained” geometries in **TS1**. On the other hand,  $E_{\text{int}}$  is known as the *interaction energy* and represents the energy gain arising from the interaction between the Au and Rh fragments in **TS1**. This analysis revealed that  $E_{\text{dist}}$  for the Au fragment is substantially larger than that for Rh (32.8 vs 23.8 kcal mol<sup>-1</sup>), while the most important energy term is  $E_{\text{int}}$  (71.3 kcal mol<sup>-1</sup>). Hence, we next decided to examine in detail the interactions involved in **TS1** via Natural Bond Orbital (NBO) and second order perturbation theory (SOPT) analyses. NBO indicates that the Rh–Au bond in **TS1** involves the electron donation of a filled *4d* orbital from Rh into an empty *6s* orbital of Au, and the back-donation of a filled *5d* orbital from Au into an anti-bonding orbital mainly constituted by a hybrid *sd* orbital from Rh (Figures 5a,b). The sum of the two (mostly the first one, see donor-acceptor interaction energies by SOPT in Figures 5a,b and Table S4) contributes to make the Rh–Au bond. NBO analysis also suggests that the Au center does not participate in the formation of the Rh–Pf bond. This interaction is initiated instead by electron donation from a hybrid *sp* orbital of the Pf group to an empty hybrid *sd* orbital from Rh (Figure 5c). In short, our analysis supports that the formation of the Rh–Au bond using electron density from Rh prepares the formation of the Pf–Rh bond by polarizing the electron density of the Au–Pf bond towards the Pf ipso carbon atom. In other words, the *oxidative addition* is the result of an *asymmetric oxidative insertion* of the electron donor Rh: into the Pf–AuL bond.

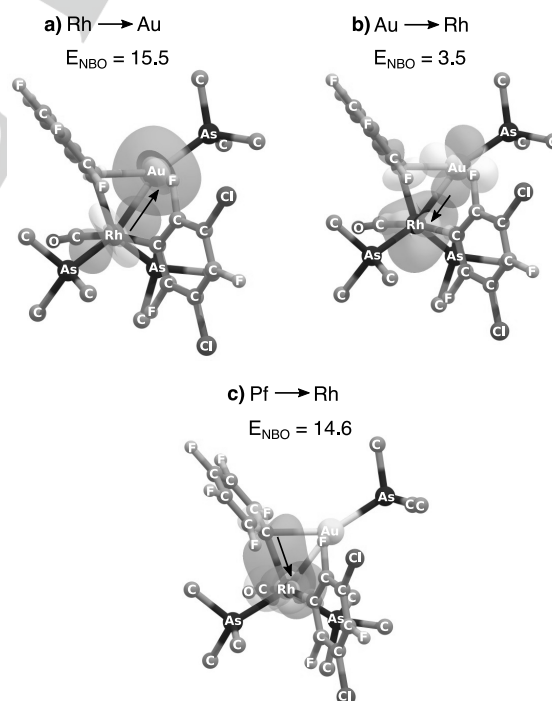


**Figure 5.** Isosurfaces (isovalue = 0.05 e<sup>-</sup> bohr<sup>3</sup>) of selected NBOs in **TS1**. Above: a)+b) electron-donation between Rh and Au to form the Rh–Au bond; it can alternatively be defined as Rh-to-Au donation (a) + Au-to-Rh back-donation (b). Below: c) electron donation from the Pf group forming the C–Rh bond, while breaking the C–Au bond. Donor-acceptor interactions in each NBO,  $E_{\text{NBO}}$  (in kcal mol<sup>-1</sup>), obtained from second order perturbation theory (SOPT) are also presented. H atoms are omitted and  $\text{AsPh}_3$  is drawn as  $\text{AsC}_3$  for better observation.

The geometrical evolution discussed above, in which two ligands in *trans* (CO and Rf) remain as mere spectators, is reminiscent of the classical oxidative addition of H<sub>2</sub> to the Vaska's type complex *trans*-[MCl(CO)(PPh<sub>3</sub>)<sub>2</sub>] (M = Rh, Ir).<sup>18</sup> In the latter, however, the L–M–L axis remains passive while the more electron poor Cl–M–CO axis undergoes angle bending;<sup>19</sup> the process involves electron donation of the electron pair of the H–H bond to Rh,<sup>20</sup> eventually leading to a different isomer when back-donation from Rh cleaves the H–H bond.<sup>21</sup>

Some concepts used in the text deserve some comment. We are using the uncommon expression *asymmetric oxidative insertion* of Rh into the Au–C bond to define the intimate oxidation/reduction mechanism of the process, at variance with the *symmetric oxidative addition* occurring with H<sub>2</sub> on Vaska's complexes. The rules to assign formal oxidation numbers impose that the M–M' bonds should not count because the electron pair in that bond is supposed to be equally shared between the two metals (non-polarized bond); with this rule, complexes **12** would be assigned Rh<sup>II</sup> and Au<sup>0</sup> oxidation states, corresponding to an overall one electron oxidation of Rh<sup>I</sup> by Au<sup>I</sup>. In the latter section we have considered the anionic moiety [(Ph<sub>3</sub>As)Au:]<sup>-</sup> because classifying ligands in a *trans-influence* list requires to consider them as 2e<sup>-</sup> donors; within this approach, the complexes would be assigned Rh<sup>III</sup> and Au<sup>-1</sup>. Finally, in apparent contradiction, in **TS1** the Pf–AuL bond is eventually asymmetrically cleaved providing the Rh center with the fragments LAu<sup>+</sup> and Pf<sup>-</sup>. This illustrates how assigning oxidation states may be misleading about the real electron density on the metal, and about bond polarizations. This is better examined by looking at the NPA (natural population analysis) charges on Rh in **TS1** and **12** (-1.15 and -1.22 respectively), which show that Rh<sup>III</sup> has more negative charge than in the Rh<sup>I</sup> complex **2** (-0.70). Overall, Rh gains electron density while it is formally being oxidized. The gold atom shows only minor differences between the linear molecule and the octahedral intermediate, with similar slightly positive charges in the range +0.27 to +0.20.

In conclusion, the Rh<sup>I</sup>Ar/Au<sup>I</sup>Ar' transmetalation studied here does not follow the traditional Ar/Ar' double-bridged mechanism, but involves an oxidation/reduction mechanism. Moreover this is also an unusual one in that it is initiated by donation of an electron pair from Rh to Au, which eventually triggers the transfer of [Ar:]<sup>-</sup> to Rh. Interestingly, the different electronic characteristics of the polar Ar–AuL and the non-polar H–H bonds on Vaska's type complexes induce formation of different octahedral isomers.

## Experimental Section

Experimental and computational details are given in the SI.

## Acknowledgements

The authors thank the financial support from the Spanish MINECO (projects CTQ2016-80913-P and CTQ2017-89217-P), the Junta de Castilla y León (project VA051P17). The

DJEI/DES/SFI/HEA Irish Centre for High-End Computing (ICHEC) is also acknowledged for the provision of computational facilities and support. M. N. P.-D. gratefully acknowledges the Spanish MECED for a FPU scholarship.

**Keywords:** bimetallic catalysis • oxidative addition • gold • rhodium • transmetalation mechanism

- [1] a) M. H. Pérez-Temprano, J. A. Casares, P. Espinet, *Chem. –Eur. J.* **2012**, *18*, 1864–1884; b) D. R. Pye, N. P. Mankad, *Chem. Sci.* **2017**, *8*, 1705–1718.
- [2] a) Y. Shi, S. A. Blum, *Organometallics*, **2011**, *30*, 1776–1779; b) J. delPozo, J. A. Casares, P. Espinet, *Chem. – Eur. J.* **2016**, *22*, 4274–4284; c) R. J. Oeschger, P. Chen, *J. Am. Chem. Soc.* **2017**, *139*, 1069–1072.
- [3] J. delPozo, D. Carrasco, M. H. Pérez-Temprano, M. García-Melchor, R. Álvarez, J. A. Casares, P. Espinet, *Angew. Chem. Int. Ed.* **2013**, *52*, 2189–2193.
- [4] For more details and formation of homocoupling products R<sup>2</sup>–R<sup>2</sup>, see: J. del Pozo, G. Salas, R. Álvarez, J. A. Casares, P. Espinet, *Organometallics*, **2016**, *35*, 3604–3611; and references therein.
- [5] M. N. Peñas-Defrutos, C. Bartolomé, M. García-Melchor, P. Espinet, *Chem. Commun.* **2018**, *54*, 984–987.
- [6] D. Carrasco, M. García-Melchor, J. A. Casares, P. Espinet, *Chem. Commun.* **2016**, *52*, 4305–4308.
- [7] A. L. Casado, P. Espinet, *Organometallics*, **1998**, *17*, 3677–3683.
- [8] The reaction rate when the products formed reaches 10% is proportional to (0.90)<sup>2</sup> – (0.10)<sup>2</sup> ≈ 0.8. At that point the rate has decreased to 80% of r<sub>0</sub>. The rate constant error within this limit, when translated to ΔG<sup>‡</sup> values, is < 1 kcal mol<sup>-1</sup>.
- [9] These experiments were carried out at 298 K due to the lower rate in the presence of high concentrations of free arsine.
- [10] For a related case of arsine dependence in Pd see: M. H. Pérez-Temprano, J. A. Casares, A. R. de Lera, R. Álvarez, P. Espinet, *Angew. Chem. Int. Ed.* **2012**, *51*, 4917–4920.
- [11] S. Kozuch, S. Shaik, *Acc. Chem. Res.* **2011**, *44*, 101–110.
- [12] S. Hoops, S. Sahle, R. Gauges, C. Lee, J. Pahle, N. Simus, M. Singhal, L. Xu, P. Mendes, U. Kummer, *Bioinformatics*, **2006**, *22*, 3067–3074.
- [13] To be more precise (see SI) COPASI produces changes in **12** and **13** (less than 1 kcal mol<sup>-1</sup>) when the reversibility condition is imposed.
- [14] a) C. L. McMullin, J. Jover, J. N. Harvey, N. Fey, *Dalton Trans.* **2010**, *39*, 10833–10836; b) C. L. McMullin, N. Fey, J. N. Harvey, *Dalton Trans.* **2014**, *43*, 13545–13556.
- [15] R. Asatryan, E. Ruckenstein, J. Hachmann, *Chem. Sci.* **2017**, *8*, 5512–5525.
- [16] For a related case see: C. Bartolomé, Z. Ramiro, M. N. Peñas-Defrutos, P. Espinet, *ACS Catal.* **2016**, *6*, 6537–6545.
- [17] a) S. I. Gorelsky, D. Lapointe, K. Fagnou, *J. Am. Chem. Soc.* **2008**, *130*, 10848. b) M. García-Melchor, S. I. Gorelsky, T. K. Woo, *Chem. – Eur. J.* **2011**, *17*, 13847–13853; c) F. M. Bickelhaupt, K. N. Houk, *Angew. Chem. Int. Ed.* **2017**, *56*, 10070–10086.
- [18] L. Vaska, J. W. DiLuzio, *J. Am. Chem. Soc.*, **1962**, *84*, 679–680.
- [19] C. E. Johnson, R. Eisenberg, *J. Am. Chem. Soc.* **1985**, *107*, 3148–3160.
- [20] A. Didieu, A. Strich, *Inorg. Chem.* **1979**, *18*, 2940–2943.
- [21] J. J. Low, W. A. Goddard III, *J. Am. Chem. Soc.* **1984**, *106*, 6928–6937.

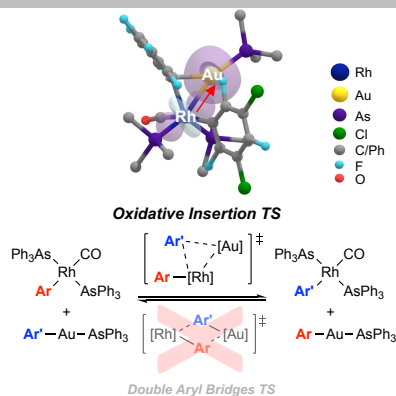
## Entry for the Table of Contents (Please choose one layout)

Layout 1:

## COMMUNICATION

Text for Table of Contents

Nucleophilic attack of Rh(I) to gold triggers the asymmetric oxidative insertion of Rh into the Au–Aryl bond, which is the unexpected mechanism behind the Aryl/Aryl' exchange between the two metals.



M. N. Peñas-Defrutos, C. Bartolomé,\*  
M. García-Melchor,\* P. Espinet\*

Page No. – Page No.

**Rh<sup>I</sup>Ar/Au<sup>I</sup>Ar' Transmetalation, a Case of Group Exchange Pivoting on Formation of M–M' Bonds via Oxidative Insertion**

Layout 2:

## COMMUNICATION

Author(s), Corresponding Author(s)\*

Page No. – Page No.

Title

Text for Table of Contents

22

22